Experimental and theoretical study of quantized spin-wave modes in micrometer-size permalloy wires

Y. Roussigné,* S. M. Chérif, C. Dugautier, and P. Moch
CNRS, Laboratoire PMTM (UPR 9001), Université Paris-Nord, 93430 Villetaneuse, France
(Received 8 September 2000; revised manuscript received 13 November 2000; published 14 March 2001)

Using Brillouin light scattering measurements, we have studied the properties of the spin waves in various arrays of Permalloy wires showing widths of 0.5, 1, and 1.5 μm. When the transferred in-plane wave vector $\boldsymbol{\kappa}_{\parallel}$, specified by the experimental setup, is perpendicular to the wires, a sampling of the Damon-Eshbach surface mode branch giving rise to a set of discrete dispersionless modes is observed. We attribute this behavior to a lateral quantization of the wave vector $\mathbf{q}_{\parallel}$ of the magnetic excitations. The frequency separation between two adjacent modes is found to decrease when the width D of the wires increases. However, this frequency dependence does not simply follow the expected one assuming the usual naive relation $q_{\parallel,n}=n\pi/D$, which would not allow one to give account of the behavior of the lowest mode $n=0$. We have performed numerical calculations of the dynamical magnetization response functions of these rectangular cross section wires using the method of finite elements. The magnetic parameters used in these calculations were derived from the experimental Brillouin spectra of the unpatterned films. Both our experiments and our calculations agree with the results expected from the unpatterned film assuming the following discrete values: $q_{\parallel,0}=0$, $q_{\parallel,n}=\pi(n+\beta)/D$. The zero value observed for the lowest mode $n=0$ simply results from the calculation and does not need for an additional hypothesis as previously proposed.

DOI: 10.1103/PhysRevB.63.134429 PACS number(s): 75.40.Gb, 79.60.Jv, 78.35.+c

I. INTRODUCTION

In the last decade potential applications in magnetic storage devices and sensors[1,2] and the availability of fabrication techniques[3–7] have increased the interest of the study of both static[1,2,8] and dynamic[9–13] magnetic properties of micron-scale-size elements. From a more fundamental point of view, periodic arrays of micron-size-wide wires or dots are good candidates to point out the striking physical changes induced by the reduction of the dimensionality compared to two-dimensional infinite layers. For instance, the study of the high-frequency dynamic properties of such arrays using the Brillouin light scattering (BLS) technique allows one to derive basic information about the parameters monitoring their magnetic properties such as magnetic anisotropy[10,11,14] or the size-dependent demagnetizing field[10,11,15] throughout the investigation of the long-wavelength spin waves propagating in these reduced systems. In laterally confined magnetic structures, if the involved in-plane wave vector is parallel to the reduced dimension and is associated with a wavelength comparable to the size of the object under investigation, the observed spin waves are expected to be satisfactorily described by the quantization of the wave vector $\mathbf{q}_{\parallel}$, which specifies the magnetic modes of the continuous film.[9,16] This generates a sampling of the magnetostatic surface mode branch [so-called Damon-Eshbach (DE) mode] in a set of discrete, dispersionless magnetic excitations associated with discrete values $q_{\parallel,n}$ of the modulus $q_{\parallel}$ of $\mathbf{q}_{\parallel}$. However, in the case of a strong magnetic anisotopy and of a broad experimental DE linewidth in the continuous film, observed, for instance, in cobalt, such quantization effects are smeared out.[17] In contrast, Permalloy appears to be a good candidate to investigate them because of its negligible anisotropy and of the sharpness of the observed magnetic Brillouin lines in this material. In the case of wire arrays, if the thickness d of each wire is small enough compared to its width D, the frequencies of the quantized modes can be estimated by inserting the usual discrete values of $q_{\parallel}$ ($q_{\parallel,n}=n\pi/D$, where n is an integer) into the well-known relation providing for the frequencies of the DE mode of a continuous layer in the dipolar approximation and in the absence of anisotropy.[18] However, this model is approximate and an exact calculation of the eigenfrequencies is necessary to allow a rigorous interpretation of the experimental results. To our knowledge up to date, the few published theoretical studies describing the spin waves in wires only concerned axially magnetized cylinders showing an elliptical cross section and used the dipolar approximation in the absence[19] or, rather recently, in the presence of anisotropy.[20] But there are no published calculations of the spin-wave spectrum in a ferromagnetic wire showing a rectangular cross section. This is one of the points that we treat in this paper. The derivation of the frequencies of the eigenmodes using a complete numerical approach, in the absence of exchange, is achieved and compared to our BLS experimental results obtained on a set of uncoupled permalloy wires showing various widths. The investigation of different arrays also allowed us to study the dependence of the quantized modes frequencies upon the width D of the wires. This information was missing in previously reported works dealing with the experimentally observed spin-wave quantization, since only a single value of width was investigated.[9,16] A more rigorous quantization condition for the in-plane wave vector is presented and compared to the usual naive correspondence ($q_{\parallel,n}=n\pi/D$) based on resonance geometrical conditions.

II. EXPERIMENT

The native sample consisted of a $d=29$ nm thick Permalloy layer deposited on a Si(100) wafer. The wire arrays were

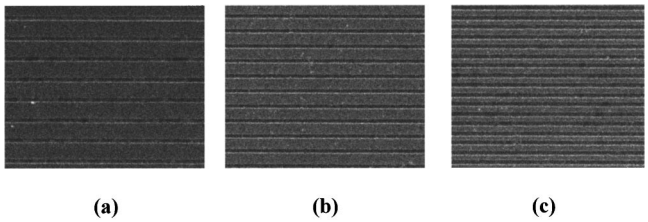

FIG. 1. SEM micrographs of Permalloy wires arrays: (a) 1.5 μm width, (b) 1 μm width, and (c) 0.5 μm width.

fabricated utilizing electron beam lithography and ion beam sputtering. First, a resist mask is realized by irradiation of a 100-nm-thick methyl-methacrylate (PMMA) film in a scanning electron microscope (SEM). The irradiated resist is then removed using a soft chemical solution, and the sample is mounted in a ultrahigh-vacuum chamber where the realized masks are transferred into the magnetic layer using an Ar^+ ion beam sputtering. Finally, the remaining resist is removed in trichloroethylene and the engraved structure is controlled by SEM observation. The details of our fabrication method are presented elsewhere.[7] The prepared patterned structures consisted of three periodic arrays of 0.3-μm-spaced wires with widths D of (a) 1.5 μm, (b) 1 μm, and (c) 0.5 μm, respectively. Figure 1 shows a SEM image of these studied wires. The patterned areas were $500\,\mu\text{m}\times 500\,\mu\text{m}$, which is enough to allow Brillouin measurements, since the laser beam is focused on an area of about 100 μm diameter. An unpatterned area undergoing all the fabrication process was maintained on the layer in order to compare its BLS spectra to those of the arrays.

The BLS measurements were performed at room temperature using a Sandercock-type (2×3)-pass tandem Fabry-Pérot interferometer characterized by a contrast ratio higher than 10^{10} and by a finesse of 100. For typically used geometrical conditions, this finesse corresponds to the instrumental linewidth at half maximum [full width at half maximum (FWHM)] of 0.15 GHz observed for the elastically scattered light; the magnetic Brillouin lines obtained in our Permalloy structures are broader (FWHM around 0.5 GHz). Anyway, this broadening, which is probably due to dissipative terms difficult to evaluate, is significantly smaller than in the case of cobalt patterned films, as pointed out in the Introduction. The samples were illuminated by a single-mode Ar^+ ion laser, using a power of 50 mW at the wavelength $\lambda = 5145$ Å. Cross polarizations between the incident and scattered beams were used in order to practically suppress the light scattered by phonons: as well known, in metallic films the main contribution to phonon scattering arises from the ripple mechanism at the surface,[21] which, at least in the absence of optical anisotropy at the laser wavelength, cancels for cross polarizations; a small additional elasto-optic contribution is sometimes observed,[22] but with cross polarizers, it is too weak to give rise to a measurable intensity. The backscattering geometrical setup was chosen such as the in-plane transferred wave vector $\kappa_\parallel$ remained perpendicular to the external magnetic field **H** applied along the wire axes. The variations of the Brillouin spectra versus $\kappa_\parallel$ are derived from their study versus the angle θ between the incident illuminating beam and the direction normal to the plane of the thin layer; θ could be swept by rotating the sample around an in-plane axis parallel to **H**. The amplitude of $\kappa_\parallel$ is related to the angle of incidence θ by the relation $\kappa_\parallel = (4\pi/\lambda)\sin\theta$; its order of magnitude is about $10^5\,\text{cm}^{-1}$. This special attention to the behavior of the spectra versus the difference between the wave vectors of the incident illuminating beam and of the scattered collected beam (more specifically of their projections parallel to the films) provided for rather precise dispersion curves in the case of continuous films: in this case, indeed, we simply have to apply the conservation law $\mathbf{q}_\parallel = \boldsymbol{\kappa}_\parallel$. As discussed below, for patterned structures we derived pseudodispersion curves. Finally, the sample could be rotated around an axis normal to the layer, allowing a variation of the directions of $\boldsymbol{\kappa}_\parallel$ (and of **H**) with respect to the orientation of the wires.

III. RESULTS AND DISCUSSION

A. Eigenfrequencies in rectangular cross section wires

The theoretical study of the spin-wave magnetic excitations in structured layers is complicated so as, to date, the literature is still poor in this field. An expression describing the spin-wave modes in an axially magnetized cylinder with an elliptical cross section, using the dipolar approximation and in the absence of anisotropy and of exchange, has been derived by De Wames and Wolfram[19] and we have generalized it for nonzero uniaxial anisotropy.[20] However, a rigorous quantitative analysis of the spin-wave spectrum of wires showing a rectangular cross section, which is the case of the presently studied wire arrays, cannot use these former results. Below, we present a completely numerical approach based on the resolution, using the finite-elements method, of the equations characterizing the spin waves in order to calculate the impulse responses. These responses are related to the amplitudes of the existing spin waves through the fluctuation dissipation theorem and then enable us to evaluate the frequencies of the eigenmodes. Indeed, since we were interested in comparing our numerical results to experimental data obtained with $\boldsymbol{\kappa}_\parallel$ perpendicular to the wire, we seeked for functions independent of the position z along the wire (in the general case, the translational invariance along z allows one to define a one-dimensional wave vector for any excitation: in the studied case, the canceling of this wave vector results from conservation laws for $\boldsymbol{\kappa}_\parallel$ perpendicular to the wire).

We have calculated the frequencies in the dipolar approximation. In this case, the Landau-Lifshitz equation can be written in the absence of anisotropy as

$$i\frac{\omega}{\gamma}\mathbf{m} = \mathbf{m}\times\mathbf{H} + \mathbf{M}\times\mathbf{h}, \tag{1}$$

where ω is the angular frequency, γ is the gyromagnetic factor, **m** is the oscillating magnetization, **M** is the static magnetization, **H** is the applied field, and **h** is the oscillating demagnetizing field.

Inside the magnetic wire,

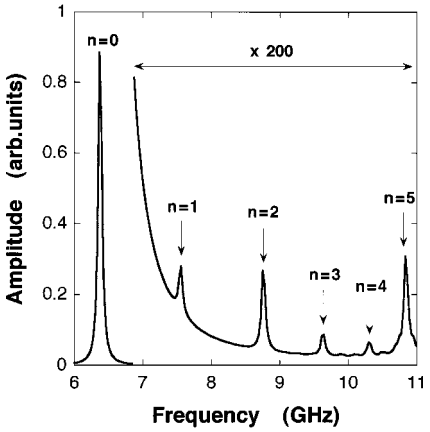

FIG. 2. Calculated response function for wires showing a rectangular cross section characterized by a thickness $d=29$ nm and a width $D=1$ μm. The external magnetic field, equal to 550 Oe, is applied parallel to the wires axis. $4\pi M=7.8$ kOe, $\gamma=1.87\times10^7$ Hz/Oe. The eigenmodes are labeled by an integer $n\geqslant 0$.

$$\mathbf{b}=\mathbf{h}+4\pi\mathbf{m}. \tag{2}$$

Outside the magnetic wire,

$$\mathbf{b}=\mathbf{h}. \tag{3}$$

Moreover,

$$\nabla\cdot\mathbf{b}=0, \quad \nabla\times\mathbf{h}=\mathbf{0}. \tag{4}$$

In the magnetostatic approximation, one introduces a potential Φ in order to replace $\mathbf{h}$ by $\nabla\Phi$ inside the magnetic wire, and a potential Ψ in order to replace $\mathbf{h}$ by $\nabla\Psi$ outside the magnetic wire.

The boundary conditions derive from the continuities of the tangential components of $\mathbf{h}$ and of the normal component of $\mathbf{b}$:

$$\nabla\Phi\times\mathbf{n}=\nabla\Psi\times\mathbf{n}, \quad \nabla\Phi\cdot\mathbf{n}+4\pi\mathbf{m}\cdot\mathbf{n}=\nabla\Psi\cdot\mathbf{n}, \tag{5}$$

where $\mathbf{n}$ is a unit vector normal to the surface of the magnetic wire.

In order to obtain the appropriate response functions, we add a local probe field $\mathbf{h}_p$ to $\mathbf{h}$: at any point, the response $\mathbf{m}$ is a function of ω. The eigenfrequencies correspond to the maxima of the amplitude of the response. The detail of the numerical calculation is presented in the Appendix.

Figure 2 displays an example of an appropriate correlation function related to the spectra corresponding to the thickness $d=29$ nm and to a width D of 1 μm. The amplitude of the response depends on the excitation point: however, the positions of the maxima are always at the same frequencies. Each calculated frequency is labeled by an integer $n\geqslant 0$. The magnetic parameters (see figure caption) one has to know are the saturation magnetization M and the gyromagnetic factor γ. They were deduced from the fit of the experimental dispersion curve of the infinite layer as shown in the next paragraph. The taken H value in the calculations corresponds to the experimentally measured one using a calibrated probe. The calculated frequencies of the quantized modes are reported in Table I. Notice that the frequency of the lowest mode $(n=0)$ does not depend on the width of the wires. This is not surprising: it corresponds to a well-known bulk mode of the unpatterned continuous film, which shows the frequency

$$\omega=\gamma[H(H+4\pi M)]^{1/2}. \tag{6}$$

On the other hand, the frequency separation between two adjacent quantized modes increases when the width D of the wires decreases. Also notice that, for a given width, the frequency separation is a decreasing function of n.

In previous works,[16,23] the frequencies of the quantized modes were estimated by inserting discrete values $q_{\parallel,n}$ of the surface wave vector $q_\parallel$ into the relation providing for the frequencies of the DE mode of a continuous layer in the dipolar approximation and in the absence of anisotropy. For an infinite layer of thickness d, this frequency is given by[18]

$$\omega=\gamma[H(H+4\pi M)+(2\pi M)^2(1-e^{-2q_{\parallel,d}})]^{1/2}. \tag{7}$$

In order to fit our obtained frequencies to the values which would result from Eq. (7) using an appropriate quantization of the wave vector, it is convenient to define Γ_n,

$$\Gamma_n=\ln\left[\frac{(2\pi M)^2}{(H+2\pi M)^2-(\omega_n/\gamma)^2}\right], \tag{8}$$

and to evaluate Γ_n for each numerically calculated frequency. In Fig. 3, we report Γ_n as a function of the integer n for the (a) $D=0.5$ μm, (b) $D=1$ μm, and (c) $D=1.5$ μm wide wires. It can be easily noticed from Eqs. (7) and (8) that Γ_n can be identified with $2q_{\parallel,n}d$ where $q_{\parallel,n}$ is an *ad hoc* equivalent wave vector. The analysis of Fig. 3 shows that, for the three wire arrays and for $n\neq 0$, we obtain a relation

$$\Gamma_n=\alpha(n+\beta), \tag{9}$$

TABLE I. Comparison of the calculated and measured frequencies in the Permalloy (29-nm) wire arrays for $H=550$ Oe applied parallel to the wires axis and $\boldsymbol{\kappa}_\parallel$ perpendicular to it. Calculations using $4\pi M=7.8$ kOe and $\gamma=1.87\times10^7$ Hz/Oe (values experimentally derived from the continuous film).

	$n=0$		$n=1$		$n=2$		$n=3$		$n=4$	
	Calc.	Expt.	Calc.	Expt.	Calc.	Expt.	Calc.	Expt.	Calc.	Expt.
0.5 μm	6.37	6.45	8.42	8.4	10.12	10.2	11.13	11.15		
1 μm	6.37		7.56	7.42	8.75	8.63	9.64	9.65	10.3	10.33
1.5 μm	6.37		7.2	7.18	8.13	8.07	8.84	8.8	9.46	9.4

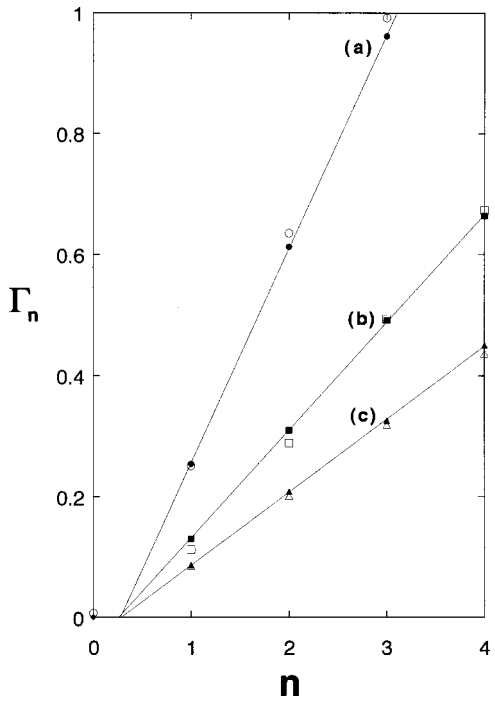

FIG. 3. Γ_n as a function of n (see text): (a) 0.5-μm-wide wires, (b) 1-μm-wide wires, and (c) 1.5-μm-wide wires. From measurements: open symbols. From numerical calculations: solid symbols. The quantization condition can be related to the effective wave vector involved in a continuous layer obeying $q_{\parallel,n}=(\pi/D)(n+\beta)$, except at $n=0$, for which $q_{\parallel,0}=0$. The lines exhibit a linear variation versus n.

where α is equal to 0.354, 0.178, and 0.121, respectively, for the 0.5-, 1-, and 1.5-μm-wide wires. This provides us with an excellent approximation

$$\alpha=2\pi\frac{d}{D}. \tag{10}$$

Moreover, β was found to be constant in the wires studied. The quantization condition can then be related to an effective wave vector of the infinite layer obeying

$$q_{\parallel,n}=\frac{\Gamma_n}{2d}=\frac{\pi}{D}(n+\beta), \tag{11}$$

where apparently β is nearly equal to $-\frac{1}{3}$.

Our calculations show that the quantization condition does not require additional hypotheses in contrast with previously published interpretations,[23] where Rado-Weertman conditions have been invoked. Finally, a simple interpretation based on resonance geometrical conditions is approximately valid.

Now let us focus on the lowest mode $n=0$: it corresponds to $\Gamma_0=0$, which means that it is associated with $q_{\parallel,0}=0$. It is interesting to notice that $\omega_1-\omega_0$ is found to be reduced compared to the difference related to a wave vector separation of π/D, which would result from the application of expression (11) to $n=0$ as well as to $n=1$. This reduction is experimentally observed, as reported in the next paragraph. Such a peculiarity of the mode $n=0$ has been experimentally observed elsewhere:[16,23] it was attributed to pinning conditions or, alternatively, derived from approximate anterior calculations concerning the uniform modes in wires.[24] To obtain the correct result, we do not need such more or less justified approximations.

B. Experimental study

As a result of the above described geometrical arrangement, if $\mathbf{k}_{i\parallel}$ denotes the projection of the wave vector of the incident illuminating beam on the film surface, the observed excitations in the continuous film are characterized by a wave vector $\mathbf{q}_\parallel=\pm\kappa_\parallel=\pm 2\mathbf{k}_{i\parallel}$ (with indeed $\kappa_\parallel=4\pi\sin\theta/\lambda$). Concerning the selection rules for Brillouin scattering, the usual wave vector conservation law is no longer meaningful for finite sizes: one then expects to observe a discrete spectrum consisting of the sampling of the DE mode branch in a few lines related to quantized values of the in-plane wave vector. Strictly speaking, in a wire one can only specify a one-dimensional wave vector for the observed excitations, which is equal to 0 in the present case. However, one suspects that the characteristics of the involved spin waves show reminiscences of the magnons propagating in an infinite continuous layer with a wave vector $\mathbf{q}_\parallel$: more specifically, the Brillouin line intensity corresponding to each magnetic mode, is expected to be related to its $q_{\parallel,n}$ value, defined above through Eqs. (8) and (11), and, consequently, to be non-negligible only for $\kappa_\parallel$ lying in the neighborhood of $q_{\parallel,n}$. This intensity then depends upon θ and presents a maximum at θ_M where $\sin\theta_M=(\lambda/4\pi)q_{\parallel,n}$. We have recently derived a semiquantitative model of the $\kappa_\parallel$ dependence of the Brillouin spectra in wires.[17]

It is important to recall here that, in addition to the discussed dipolar modes, there also exist exchange modes (often called standing spin waves), the characteristics of which strongly depend upon the thickness of the samples and upon the magnetic exchange value: for the chosen thickness ($d=29$ nm), they lie at frequencies significantly higher than the lines studied in this paper. We observed the first standing mode around 18 GHz as expected. They are not present in the spectra in this paper and will not be discussed in the following.

Figure 4 shows the anti-Stokes sides of BLS spectra of the unpatterned film and of the 1.5-μm-wide wires obtained with $H=550$ Oe and $\theta=11°$ (i.e., $\kappa_\parallel=0.46\times10^5$ cm^{-1}). In order to increase the signal-to-noise ratio, the scanning speed of the Fabry-Pérot interferometer was reduced by a factor of 10 in the frequency region of interest. One can see that the usual DE line of the infinite continuous layer [Fig. 4(a)] is replaced in the patterned structure [Fig. 4(b)] by two well-separated lines. This splitting is directly connected to the quantization induced by the finite width D: in the experimental conditions studied, only two modes (associated with two distinct values of n corresponding to values of $q_{\parallel,n}$ in the vicinity of the imposed $\kappa_\parallel$) show a measurable intensity. To ensure that such quantized discrete modes are originating from the finite width of the wires, we have investigated their frequencies versus the angle of incidence. To illustrate this study, Fig. 5

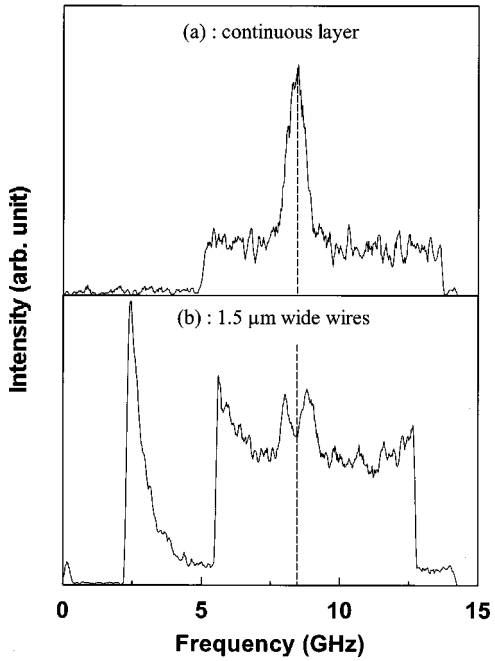

FIG. 4. Anti-Stokes parts of Brillouin spectra obtained from Permalloy (29 nm) samples. Backscattering with $\theta = 11°$, $H = 550$ Oe applied along the wires axis, and $\kappa_{\|}$ perpendicular to it: (a) unpatterned area, (b) patterned area.

displays the observed spectra on the 1-μm-wide wires array at different angles of incidence, θ. The frequencies do not depend upon θ, in contrast with the relative intensities of the lines: the lowest modes (small n) appear at low values of θ; with increasing θ, higher modes are activated, while the lowest vanish. The frequency shift between adjacent lines decreases versus n. Due to the resolving power limited by the FWHM of each line, for large n their separation cannot be put in evidence and, above an angle of incidence of about 35°, the spin-wave spectra and their variation versus θ look like the observed ones in an infinite continuous layer. An illustration of the above-mentioned features is given in Fig. 6 where we present the results obtained for (a) the native Permalloy film, (b) the 1-μm-wide wires, and (c) the 1.5-μm-wide wires. The wire arrays clearly exhibit the expected splitting of the dipolar surface line (DE mode) into a set of quantized dispersionless lines. This figure shows that the eigenfrequencies of the quantized modes depend on D and that the frequency separation between two adjacent modes decreases when D increases (and, consequently, π/D decreases).

The solid line of Fig. 6(a) provides the best fit with the experimental data of the unpatterned region recorded at $H = 0.55$ kOe: it leads to $4\pi M = 7.8$ kOe and $\gamma = 1.87 \times 10^7$ Hz/Oe (g factor: 2.01). These values are in complete agreement with the reported ones in our previous study[11] concerning square dots elaborated in the same native layer. They also rather satisfactorily agree with the published data in bulk Permalloy: $\gamma = 1.9 \times 10^7$ Hz/Oe (g factor: 2.05) and $4\pi M = 10$ kOe. Notice, however, a slight reduction of $4\pi M$ compared to the bulk, which was previously reported in thin Permalloy films.[25]

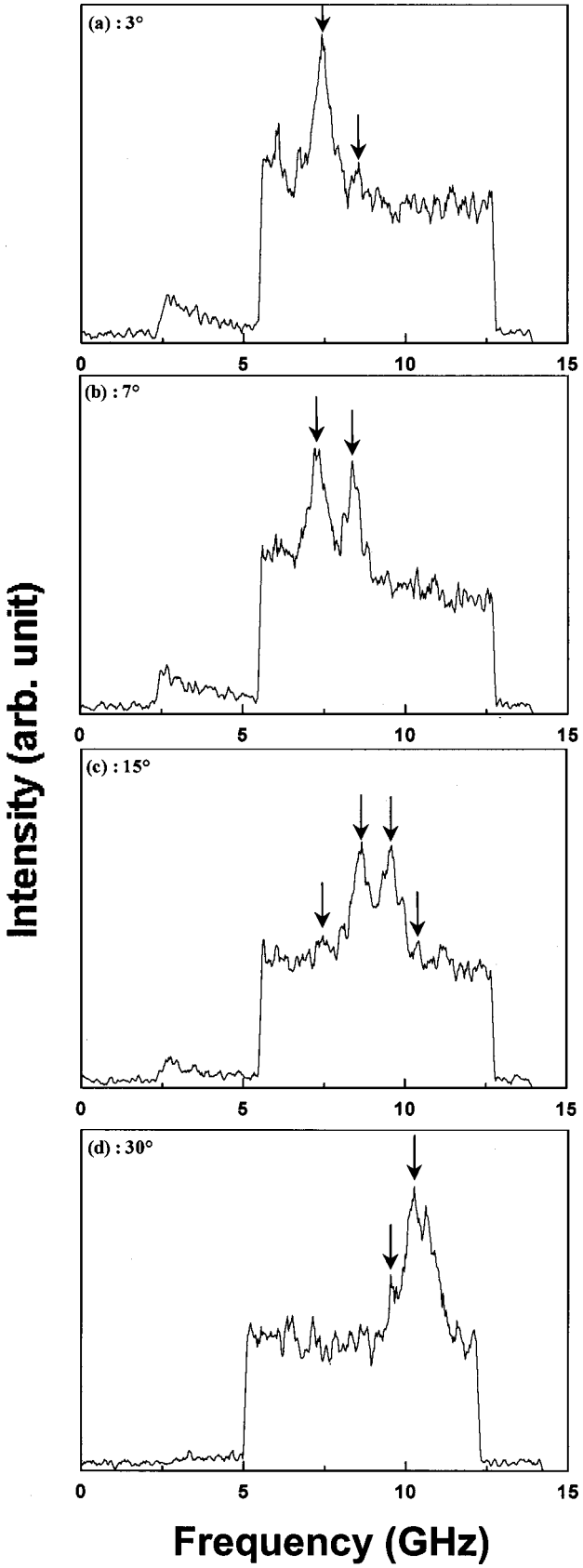

FIG. 5. Anti-Stokes parts of Brillouin spectra obtained from 1-μm-wide wires at various angles of incidence with $H = 550$ Oe applied along the wires axis and $\kappa_{\|}$ perpendicular to it. The arrows indicate the quantized modes.

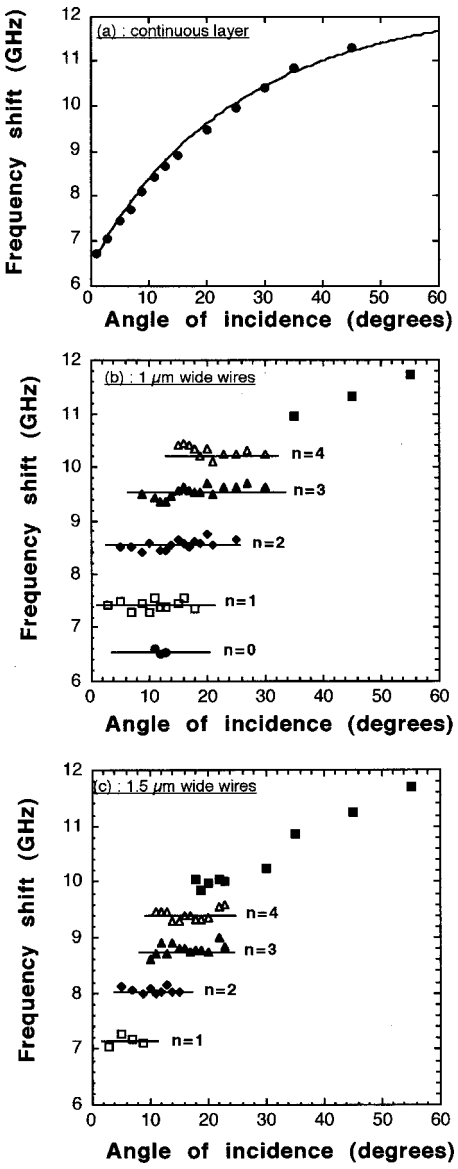

FIG. 6. Spin-wave dispersion for the Permalloy (29-nm) layer obtained with an external magnetic field $H=550$ Oe applied along the wires axis and $\boldsymbol{\kappa}_{\parallel}$ perpendicular to it: (a) continuous layer, (b) 1-μm-wide wires, and (c) 1.5-μm-wide wires. For the continuous layer, the solid line represents the best fit obtained with $4\pi M=7.8$ kOe and $\gamma=1.87\times10^{7}$ Hz/Oe. For the wires, the magnetic field is parallel to their axis and n labels the quantized modes.

Let us now focus our attention on the frequencies of the discrete modes. Experimentally, large times of accumulation were used in order to minimize errors in the determination of these frequencies. For each mode, they were measured at angles where their relative intensity is maximum in order to obtain the best available precision (see Fig. 5). The measured values of the frequencies of the observed quantized modes are reported in Table I. This table shows that the experimental and calculated values of the frequencies are in very good agreement. This is illustrated by Fig. 3, where we have reported both experimental and calculated Γ_n [derived from Eq. (8) using the experimental and the calculated values of ω_n, respectively]: the calculated quantization of $\mathbf{q}_{\parallel}$ is completely confirmed by our experimental results, and the particular behavior of the lowest mode ($n=0$) is clearly exhibited.

IV. CONCLUSION

We have fabricated patterned structures consisting of three periodic arrays of 0.3-μm-spaced Permalloy wires with widths D of 1.5, 1, and 0.5 μm, respectively. Using Brillouin light scattering measurements, we have investigated the properties of the spin waves. Special attention was paid to the behavior of the spectra versus the involved in-plane wave vector which would describe the dispersion curves in the case of continuous films. When the transferred in-plane wave vector $\boldsymbol{\kappa}_{\parallel}$, specified by the experimental setup, is perpendicular to the wires, a quantization of the DE surface mode resulting in a set of discrete dispersionless modes was observed. This was attributed to a lateral quantization of the in-plane wave vector $\mathbf{q}_{\parallel}$ of the magnetic excitations. The narrower the wires, the greater was the frequency separation between two adjacent modes. However, the quantization is more complicated than the one derived using the naive relation $q_{\parallel,n}=n\pi/D$. Our measurements, as well as our calculations for wires showing rectangular cross section using the finite-elements method, have shown that the discrete values of the in-plane effective wave vector obey the relation $q_{\parallel,n}=(\pi/D)(n+\beta)$, except for the fundamental mode ($n=0$) where $q_{\parallel,0}=0$. We have shown that the observed behavior for the lowest mode $n=0$ is not related to additional hypotheses proposed in previously published works dealing with quantization effects in arrays of Permalloy wires.

ACKNOWLEDGMENTS

The authors would like to thank Dr. H. Niedoba for providing us with the Permalloy films used in this work, Dr. S. Labbé for fruitful discussions about numerical methods, and V. Richard for his help in the sample preparation.

APPENDIX: FORMULATION OF THE FINITE-ELEMENTS METHOD

Inside the magnetic domain, we assume a static field H along the wire axis (z axis) and a probe field h_p along the x axis (x is the thickness direction); the Landau-Lifshitz relation yields

$$m_x=\frac{M[H(\partial_x\Phi+h_p)-i\Omega\,\partial_y\Phi]}{H^2-\Omega^2},$$

$$m_y=\frac{M[H\partial_y\Phi+i\Omega(\partial_x\Phi+h_p)]}{H^2-\Omega^2}, \tag{A1}$$

where Ω is the ratio ω/γ.

We introduce the coefficients p and r to write the previous relations as

$$m_x=p(\partial_x\Phi+h_p)-ir\,\partial_y\Phi,$$

$$m_y=ir(\partial_x\Phi+h_p)+p\,\partial_y\Phi. \tag{A2}$$

Thus we obtain from Eq. (2)

$$b_x=(1+4\pi p)\partial_x\Phi+4\pi p h_p-i4\pi r\,\partial_y\Phi,$$

$$b_y=(1+4\pi p)\partial_y\Phi+i4\pi r(\partial_x\Phi+h_p). \tag{A3}$$

According to Eq. (4), we derive

$$(1+4\pi p)\partial_{x^2}\Phi+(1+4\pi p)\partial_{y^2}\Phi = -4\pi p\,\partial_x h_p-i4\pi r\,\partial_y h_p. \tag{A4}$$

Outside the magnetic domain,

$$b_x=\partial_x\Psi \quad \text{and} \quad b_y=\partial_y\Psi. \tag{A5}$$

From Eq. (3) results

$$\partial_{x^2}\Psi+\partial_{y^2}\Psi=0. \tag{A6}$$

Using a parametric representation of the boundary Γ_1 between the magnetic domain and vacuum $(x(t),y(t))$, and assuming h_p to be equal to zero along the boundary, we have to write two boundary conditions (5):

$$\Phi(x(t),y(t))=\Psi(x(t),y(t)),$$

$$y'(t)[(1+4\pi p)\partial_x\Phi-i4\pi r\,\partial_y\Phi]-x'(t) \times\{[(1+4\pi p)\partial_y\Phi+i4\pi r\,\partial_x\Phi]\} =y'(t)\partial_x\Psi-x'(t)\partial_y\Psi,$$

i.e.,

$$-x'(t)(1+4\pi p)\partial_y\Phi+y'(t)(1+4\pi p)\partial_x\Phi-i4\pi r\frac{d\Phi}{dt} =-x'(t)\partial_y\Psi+y'(t)\partial_x\Psi. \tag{A7}$$

In the following, we transform the problem into an integral formulation. For any function $u(x,y)$, we derive from the boundary conditions (A7):

$$\oint_{\Gamma_1}u(x(t),y(t))[-x'(t)(1+4\pi p)\partial_y\Phi +y'(t)(1+4\pi p)\partial_x\Phi]dt -i4\pi r\oint_{\Gamma_1}u(x(t),y(t))\frac{d\Phi}{dt}dt =\oint_{\Gamma_1}u(x(t),y(t))[-x'(t)\partial_y\Psi+y'(t)\partial_x\Psi]dt. \tag{A8}$$

Using the Green relation, we can write

$$\oint_{\Gamma_1}u(x(t),y(t))[-x'(t)(1+4\pi p)\partial_y\Phi +y'(t)(1+4\pi p)\partial_x\Phi]dt =(1+4\pi p)\int\int_{\text{in}}\partial_x(u\,\partial_x\Phi)dx\,dy +(1+4\pi p)\int\int_{\text{in}}\partial_y(u\,\partial_y\Phi)dx\,dy, \tag{A9}$$

where the double integration is performed over the magnetic domain.

We develop Eq. (A9), and using Eq. (A4), we obtain

$$\oint_{\Gamma_1}u(x(t),y(t))[-x'(t)(1+4\pi p)\partial_y\Phi +y'(t)(1+4\pi p)\partial_x\Phi]dt =(1+4\pi p)\int\int_{\text{in}}\partial_x u\,\partial_x\Phi\,dx\,dy +(1+4\pi p)\int\int_{\text{in}}\partial_y u\,\partial_y\Phi\,dx\,dy-\int\int_{\text{in}}u(4\pi p\,\partial_x h_p +i4\pi r\,\partial_y h_p)dx\,dy. \tag{A10}$$

In the same way, we obtain

$$\oint_{\Gamma_2}u(y'\partial_x\Psi-x'\partial_y\Psi)dt-\oint_{\Gamma_1}u(y'\partial_x\Psi-x'\partial_y\Psi)dt =\int\int_{\text{out}}(\partial_x u\,\partial_x\Psi+\partial_y u\,\partial y\Psi)dx\,dy, \tag{A11}$$

where the double integration is performed over a finite domain around the magnetic domain. This domain admits the circle Γ_2 of radius R as an external boundary. One usually assumes the following condition:[26]

$$(y'\partial_x\Psi-x'\partial_y\Psi)=-\frac{\Psi}{R}. \tag{A12}$$

Therefore we can write

$$\oint_{\Gamma_1}u(y'\partial_x\Psi-x'\partial y\Psi)dt =-\frac{1}{R}\oint_{\Gamma_2}u\Psi\,dt-\int\int_{\text{out}}(\partial_x u\,\partial_x\Psi+\partial_y u\,\partial_y\Psi)dx\,dy. \tag{A13}$$

Finally,

$$(1+4\pi p)\int\int_{\text{in}}\partial_x u\,\partial_x\Phi\,dx\,dy +(1+4\pi p)\int\int_{\text{in}}\partial_y u\,\partial_y\Phi\,dx\,dy-\int\int_{\text{in}}u(4\pi p\,\partial_x h_p +i4\pi r\,\partial_y h_p)dx\,dy-i4\pi r\oint_{\Gamma_1}u\frac{d\Phi}{dt}dt =-\frac{1}{R}\oint_{\Gamma_2}u\Psi\,dt-\int\int_{\text{out}}(\partial_x u\,\partial_x\Phi+\partial_y u\,\partial_y\Phi)dx\,dy,$$

i.e.,

$$(1+4\pi p)\int\int_{\text{in}} \partial_x u\,\partial_x\Phi\,dx\,dy + (1+4\pi p)\int\int_{\text{in}} \partial_y u\,\partial_y\Phi\,dx\,dy - i4\pi r\oint_{\Gamma_1} u\frac{d\Phi}{dt}dt + \frac{1}{R}\oint_{\Gamma_2} u\Psi\,dt + \int\int_{\text{out}} (\partial_x u\,\partial_x\Phi + \partial_y u\,\partial_y\Phi)dx\,dy = \int\int_{\text{in}} u(4\pi p\,\partial_x h_p + i4\pi r\,\partial_y h_p)dx\,dy. \quad \text{(A14)}$$

This latest equation enables us to transform the initial problem into a linear system of equations: one divides the magnetic domain and the outside domain into a set of triangles; one expands the functions Φ and Ψ as linear combinations of elementary functions u_k equal to 1 at the vertex k and equal to zero at the nearest vertices; inside the triangle klm, the function $u_k(x,y)$ is equal to $a_{klm}+b_{klm}x+c_{klm}y$, where the coefficients a_{klm}, b_{klm}, and c_{klm} are chosen so that $u_k(x_k,y_k)=1$, $u_k(x_l,y_l)=0$, and $u_k(x_m,y_m)=0$; out of the triangles containing the vertex k, the function u_k is equal to zero.

*FAX: 33 (0) 1 49 40 39 38. Electronic address: cherif@lpmtm.univ-paris13.fr

[1] A. Maeda, M. Kume, T. Ogura, K. Kuroki, T. Yamada, M. Nishikawa, and Y. Harada, J. Appl. Phys. **76**, 6667 (1994).
[2] J. F. Smyth, S. Schultz, D. R. Fredkin, D. P. Kern, S. A. Rishton, H. Schmid, M. Cali, and T. R. Koehler, J. Appl. Phys. **69**, 5262 (1991).
[3] R. M. H. New, R. F. W. Pease, and R. L. White, J. Vac. Sci. Technol. B **12**, 3196 (1994).
[4] F. Rousseaux, A.-M. Hagiri-Gosnet, Y. Chen, M.-F. Ravet, and H. Launois, J. Phys. IV **4**, 237 (1994).
[5] M. Wendel, S. Kühn, H. Lorentz, J. P. Kothauss, and M. Holland, Appl. Phys. Lett. **65**, 1775 (1994).
[6] J. P. Spallas, A. M. Hawryluk, and D. R. Kania, J. Vac. Sci. Technol. B **13**, 1973 (1995).
[7] S. M. Chérif and J.-F. Hennequin, J. Magn. Magn. Mater. **165**, 504 (1997).
[8] T. Aign, P. Meyer, S. Lemerle, J. P. Jamet, J. Ferré, V. Mathet, C. Chappert, J. Gierak, C. Vieu, F. Rousseaux, H. Launois, and H. Bernas, Phys. Rev. Lett. **81**, 5656 (1998).
[9] B. A. Gurney, P. Baumgart, V. Speriosu, R. Fontana, A. Patlac, T. Logan, and P. Humbert (unpublished).
[10] B. Hillebrands, C. Mathieu, M. Bauer, S. O. Demokritov, B. Bartenlian, C. Chappert, D. Decanini, and F. Rousseaux, J. Appl. Phys. **81**, 4993 (1997).
[11] S. M. Chérif, C. Dugautier, J.-F. Hennequin, and P. Moch, J. Magn. Magn. Mater. **175**, 228 (1997).
[12] A. Ercole, A. O. Adeyeye, J. A. C. Bland, and D. G. Hasko, Phys. Rev. B **58**, 345 (1998).
[13] M. Grimsditch, Y. Jacard, and I. K. Schuller, Phys. Rev. B **58**, 11 539 (1998).
[14] R. P. Cowborn, D. K. Kolstov, A. O. Adeyeye, and M. E. Welland, Europhys. Lett. **48**, 221 (1999).
[15] S. M. Chérif, Y. Roussigné, P. Moch, J.-F. Hennequin, and M. Labrune, J. Appl. Phys. **85**, 5477 (1999).
[16] C. Mathieu, J. Jorzick, A. Frank, S. O. Demokritov, A. N. Slavin, and B. Hillebrands, Phys. Rev. Lett. **81**, 3968 (1998).
[17] S. M. Chérif, Y. Roussigné, C. Dugautier, and P. Moch, J. Magn. Magn. Mater. **222**, 337 (2000).
[18] R. W. Damon and J. R. Eshbach, J. Phys. Chem. Solids **19**, 308 (1961).
[19] R. E. De Wames and T. Wolfram, Appl. Phys. Lett. **16**, 305 (1970).
[20] S. M. Chérif, Y. Roussigné, and P. Moch, Phys. Rev. B **59**, 9482 (1999).
[21] R. Loudon and J. R. Sandercock, J. Phys. C **13**, 2609 (1980).
[22] L. Bassoli, F. Nizzoli, and J. R. Sandercock, Phys. Rev. B **34**, 1296 (1986).
[23] J. Jorzick, S. O. Demokritov, C. Mathieu, B. Hillebrands, B. Bartenlian, C. Chappert, F. Rousseaux, and A. N. Slavin, Phys. Rev. B **60**, 15 194 (1999).
[24] C. Kittel, Phys. Rev. **73**, 155 (1948).
[25] N. Bouterfas, Ph.D. thesis, Université Paris-Sud, Orsay, 1996.
[26] R. Djellouli, C. Farhat, A. Macedo, and R. Tezaur, J. Comput. Acoust. **8**, 81 (2000).